

RESEARCH ARTICLE

Open Access



Immunodynamic axis of fibroblast-driven neutrophil infiltration in acute pancreatitis: NF- κ B–HIF-1 α –CXCL1

Qiang Wang^{1,2†}, Xiao Zhang^{1†}, Chenglong Han^{1†}, Zhenyi Lv², Yi Zheng², Xuxu Liu², Zhiwei Du², Tianming Liu², Dongbo Xue^{2*}, Tao Li^{1*} and Liyi Wang^{2*} 

[†]Qiang Wang, Xiao Zhang, and Chenglong Han contributed equally.

*Correspondence: xuedongbo@hrbmu.edu.cn; litao7706@163.com; wangliyi@hrbmu.edu.cn

¹ Department of General Surgery, Qilu Hospital of Shandong University, Jinan, China

² Department of General Surgery, The First Affiliated Hospital of Harbin Medical University, Harbin, China

Abstract

Background: Acute pancreatitis (AP) is a sterile inflammation, and 10–20% of cases can progress to severe acute pancreatitis (SAP), which seriously threatens human life and health. Neutrophils and their extracellular traps (NETs) play an important role in the progression of AP. However, the immunodynamic factors between the excessive infiltration of neutrophils during the occurrence of AP have not been fully elucidated.

Methods: Adult male C57BL/6 J mice were selected. An AP model was induced by cerulein, and a control group was set up. Single-cell sequencing technology was used to reveal the cell atlas of AP pancreatitis tissue. In vivo, the model mice were treated with anti-Ly6G antibody, DNase I, SC75741, PX-478, and SRT3109 respectively. In vitro, human pancreatic stellate cells were treated with hypoxia, H₂O₂, NAC, and JSH-2, and co-cultured with neutrophils in Transwell chambers. The severity of inflammation was evaluated, and the molecular mechanism by which fibroblasts exacerbate AP was revealed through techniques such as cell colony formation assay, cell migration assay, cell transfection, immunofluorescence, flow cytometry, Western blot, reverse-transcription quantitative polymerase chain reaction (RT-qPCR), and co-immunoprecipitation (co-IP).

Results: The study showed that the elimination of neutrophils and NETs could significantly improve AP. Single-cell RNA sequencing (scRNA-seq) indicated that both neutrophils and fibroblasts in pancreatic tissue exhibited heterogeneity during AP. Among them, neutrophils highly expressed CXCR2, and fibroblasts highly expressed CXCL1. Further experimental results demonstrated that the infiltration of neutrophils in the early stage of AP was related to the activation of fibroblasts. The activation of fibroblasts depended on the nuclear factor kappa B (NF- κ B) signaling pathway induced by hypoxia. NF- κ B enhanced the activation of pancreatic stellate cells (PSCs) and the secretion of CXCL1 by directly promoting the transcription of HIF-1 α and indirectly inhibiting PHD2, resulting in the accumulation of HIF-1 α protein. The NF- κ B–HIF-1 α signal promoted the secretion of CXCL1 by fibroblasts through glycolysis and induced the infiltration of neutrophils. Finally, blocking the NF- κ B–HIF-1 α –CXCL1 signaling axis in vivo reduced the infiltration of neutrophils and improved AP.

Conclusions: This study, for the first time, demonstrated that activation of fibroblasts is one of the immunological driving factors for neutrophil infiltration and elucidated that glycolysis driven by the NF- κ B–HIF-1 α pathway is the intrinsic molecular mechanism by which



fibroblasts secrete CXCL1 to chemotactically attract neutrophils. This finding provides a highly promising target for the treatment of AP.

Keywords: Acute pancreatitis, Neutrophils, NETs, Fibroblasts

Introduction

Acute pancreatitis (AP) is a sterile inflammation, being a local immune inflammatory reaction caused by the early activation of pancreatic enzymes and subsequent autodigestion of the pancreas [1–5]. Most cases of AP are mild and can heal spontaneously, but still 10–20% of cases can progress to severe acute pancreatitis (SAP), with obvious pancreatic tissue necrosis, excessive activation of immune cells, and a large release of inflammatory mediators, triggering a systemic inflammatory reaction and leading to multiple organ failure and even death of patients [6, 7]. The key to the progression of SAP is the excessive inflammatory reaction mediated by immune cells, among which neutrophils are the first to enter the damaged site [8]. Neutrophils maintain sterility at the damaged site by releasing antibacterial molecules and NETs, but they also release various enzymes and cause tissue damage [9]. Multiple studies have shown that neutrophil infiltration promotes the progression of AP. Chen et al. enhanced pancreatic injury by directly injecting neutrophils in a mouse model of acute pancreatitis induced by L-arginine [10]. Gukovskaya et al. explored the role and mechanism of neutrophil-activated trypsin activation in acute pancreatitis and found that neutrophils promote trypsin activation in the pancreas through a nicotinamide adenine dinucleotide phosphate (NADPH) oxidase-mediated pathway [11]. Sandoval et al. found that neutrophils can cause apoptotic acinar cells to transform into necrotic cells, thus exacerbating AP [12]. Neutrophils not only mediate local tissue damage in the pancreas but also cause damage to distant organs, such as acute lung injury (ALI) and acute respiratory distress syndrome (ARDS). The recruitment, adhesion/migration, and activation of neutrophils in the lungs are involved in the occurrence of ALI. By releasing pro-inflammatory and pro-apoptotic factors, they damage the basement membrane and increase the permeability of the alveolar–capillary barrier [13–15].

In recent decades, it has been discovered that neutrophils can undergo NETosis after activation. NETosis refers to the process by which neutrophils form and release neutrophil extracellular traps (NETs) after being stimulated, and this is a form of programmed cell death. The mechanisms of NETosis mainly include “suicidal” NETosis and “vital” NETosis. The former method leads to the death of neutrophils, while neutrophils can still survive in the latter method [16–18]. With the discovery of this new form of death, NETosis, research on NETs in AP has intensified. Merza et al. thoroughly explored the role of NETs in regulating the inflammatory response and pancreatic injury in AP. The research indicates that NETs derived from neutrophils are a core component of the pathophysiology of SAP, capable of promoting trypsin activation, inflammation, and tissue damage, and inhibiting neutrophil infiltration and targeting NETs are effective methods for improving local and systemic inflammation in severe AP [19]. In addition, NETs may promote the polarization of macrophages to the M1 type through the Ccl3–Ccr5 signal, thereby exacerbating AP [20].

Given the adverse effects of neutrophils and NETs in AP, it is very important to elucidate the mechanism of large-scale neutrophil infiltration in AP. However, so far, the immunodynamic factors for the excessive infiltration of neutrophils during the occurrence of AP have not been fully understood. Previous studies have shown that in early AP, damage-associated molecular patterns, adhesion molecules, and cytokines released by damaged acinar cells can mediate the infiltration of neutrophils [21]. Additionally, there is evidence that tissue-resident macrophages and mast cells also participate in the recruitment of neutrophils by increasing the permeability of local blood vessels and secreting chemotactic factors [22]. Besides acinar cells, it is unclear whether there are other immunodynamic factors driving neutrophil infiltration other than tissue-resident macrophages and mast cells. Therefore, this study aims to explore the potential immunodynamic factors for the large accumulation of neutrophils and NETs in pancreatic tissue during AP, in order to provide new treatment methods for improving AP.

Methods

Experimental animals

All animal experiments were approved by the Laboratory Animal Use and Welfare Ethics Committee of the First Affiliated Hospital of Harbin Medical University. Adult male C57BL/6 J mice (6–8 weeks old, body weight 20 ± 2 g) were purchased from Liaoning Changsheng Biotechnology Co., Ltd. in China. They had free access to food and water, were housed in a 12-h light–dark cycle environment, and were adapted for 7 days. Before modeling, the mice were fasted overnight. For the cerulein-induced acute pancreatitis model, cerulein (Sigma) was intraperitoneally injected at a dosage of 50 μ g/kg per hour for 12 h. The control group was injected with normal saline in the same way. Twenty-four hours after the first injection of cerulein, the mice were euthanized, and pancreatic tissues were collected under sterile conditions. The fresh pancreatic tissues were placed in a tissue preservation solution for single-cell sequencing, and the remaining tissues were used for other subsequent experiments. The AP model mice were respectively intraperitoneally injected with anti-Ly6G antibody (Bio X Cell) at a dose of 500 μ g, once every other day for a total of three times [23]; DNase I (1000 U/mg, Pulmozyme, 5 mg/kg, Roche, Grenzach-Wyhlen, Germany) was intraperitoneally injected 1 h before AP induction [19]. SC75741 (HY-10496) was intraperitoneally injected at a dosage of 15 mg/kg once per hour, 3 h before acute pancreatitis modeling, and the model was established immediately after the last injection. PX-478 (HY-10231, 100 mg/kg) was intraperitoneally injected 1 h before AP induction [24]. SRT3109 (HY-15462, 50 mg/kg) was intraperitoneally injected into a mouse 1 h before AP induction. SC75741, PX-478, and SRT3109 were all purchased from Shanghai MedChemExpress.

Cell culture

Human pancreatic stellate cells (CP-H024) were purchased from Wuhan Procell Life Science & Technology Co., Ltd. Cell hypoxia experiments were carried out using a three-gas incubator (37 °C, 5% carbon dioxide, 3% oxygen). The cells were treated with hydrogen peroxide (5 mM); *N*-acetylcysteine (NAC, 5 mM) was used to scavenge reactive oxygen species (ROS) in a hypoxic environment; pancreatic stellate cells (PSC) were treated with JSH-23 (HY-13982, 200 μ M) to inhibit the NF- κ B signaling pathway.

For Transwell chamber co-culture, human pancreatic stellate cells were inoculated into the lower chamber of the Transwell chamber, while neutrophils isolated from the peripheral blood of patients with acute pancreatitis were inoculated into the upper chamber. Cobalt chloride (200 μ M) was added to the medium in the lower chamber, and the cells were treated or not treated with 2-deoxyglucose (HY-13966, 10 mM). Similarly, we used mouse immortalized pancreatic acinar cells and pancreatic stellate cells to conduct co-culture experiments in hypoxic and nonhypoxic environments through Transwell co-culture chambers. We conducted co-culture experiments using immortalized mouse pancreatic acinar cells (266–6) and mouse pancreatic stellate cells (PSC) in both hypoxic and nonhypoxic environments, with the use of cerulein and Transwell co-culture chambers.

The proliferation of pancreatic stellate cells was evaluated by the cell colony formation assay. The migration ability of pancreatic stellate cells was evaluated by the cell migration assay using Transwell chambers.

Cell transfection

Using Lipofectamine 2000 (Invitrogen), cell transfection experiments were carried out for small interfering RNAs (siP65, si-HIF-1 α) or HIF1A pcDNA3.1-3xFlag-C according to the instructions of the transfection reagent. The sense strand sequence of P65 small interfering RNA is 5'-GAGUCAGAUCAGCUCCUAATT-3', and the antisense strand sequence is 5'-UUAGGAGCUGAUCUGACUCTT-3'. The sense strand sequence of HIF-1 α small interfering RNA is 5'-GGAAAGAGAGUCAUAGAAA-3', and the antisense strand sequence is 5'-UUUCUAU GACUCUCUUUCC-3'. The negative control sequence is 5'-UUCUCCGAACGUGUCACGUTT-3', and the antisense strand sequence is 5'-ACGUGACACGUUCGGAGAATT-3'.

Extraction of peripheral blood neutrophils

All blood collection experiments were approved by the volunteers and the Ethics Committee of the First Affiliated Hospital of Harbin Medical University. The peripheral blood separation kit was purchased from Tianjin Haoyang Huake Biotechnology. Neutrophils were extracted according to the instructions.

Immunofluorescence

Cell immunofluorescence staining was performed using a confocal microwell plate. The primary antibodies used included P65 antibody (3033, CST), Ki67 antibody (28,074-1-AP, Proteintech), α -smooth muscle actin (α -SMA, 14,395-1-AP, Proteintech), myeloperoxidase (MPO, 1:200, ab300650), or hypoxia-inducible factor-1 α (HIF-1 α , 228,649, abcam). For tissue paraffin blocks, sectioning was carried out first, followed by dewaxing, dehydration, permeabilization, and blocking. Subsequently, the sections were incubated with MPO (1:200, ab300650) and CITH3 (1:200, ab281584) at 4 °C. The secondary antibodies used included CoraLite 488-conjugated goat anti-rabbit IgG (H+L) secondary antibody(SA00013-2), CoraLite 594-conjugated goat anti-mouse IgG (H+L) secondary antibody(SA00013-3), or CoraLite 594-conjugated goat anti-rabbit IgG (H+L) (SA00013-4). The above three fluorescent secondary antibodies were all purchased from Proteintech. Phase-contrast and immunofluorescence images were acquired and

examined using an LSM510 Zeiss laser inverted microscope equipped with confocal optical components (Carl Zeiss Microscopy, USA). Image acquisition was controlled by Zen software (Carl Zeiss Microscopy, USA).

Multicolor immunofluorescence

The wax blocks were embedding acute pancreatic tissues, with a slice thickness of about 4 μm . The slices were then subjected to dewaxing and hydration, antigen retrieval by microwave, blocking, incubation with primary antibody, incubation with secondary antibody, fluorescence signal amplification, nuclear staining, and mounting for observation under a microscope. After single staining was completed, follow-up staining was performed starting from step 3, the blocking step. The required reagents include dimethyl sulfoxide (DMSO) (abs9184, Absin), sterile deionized water (abs9259, Absin), xylene, ethanol (100%, 95%, 70%), 10% neutral formalin, antigen retrieval solution, blocking solution, and Tris-buffered saline with 0.1% Tween 20 (TBST). The required secondary antibody reagent kit (abs50030, Absin) was purchased from Shanghai Aibixing Biotechnology Co., Ltd. The primary antibodies used were anti-COL1A1 antibody (E8F4L, CST), anti-CD177 antibody (PA598759, Invitrogen), anti-SIGLEC5 antibody (PA511675, Invitrogen), and anti-CD54 antibody (AF6088, affinity).

H&E and immunohistochemistry

Pathological scoring of pancreatitis tissues was carried out by performing hematoxylin and eosin (H&E) pathological staining on the tissues [25] (Supplementary Table 1). We detected the expression levels of CXCL1, interleukin (IL)-1 β , and interferon (IFN)- γ in pancreatic tissues by immunohistochemistry. The primary antibodies used included CXCL1 (12,335-1-AP, Proteintech), interleukin-1 β (IL-1 β , AF5103, Affinity), and interferon- γ (IFN- γ , DF6045, Affinity).

Flow cytometry for detecting ROS

The Beyotime reactive oxygen species detection kit (S0033S) was purchased. Cells were treated according to the instructions, and then flow cytometry was performed using an excitation wavelength of 488 nm and an emission wavelength of 525 nm.

Western blot and immunoprecipitation

Cell proteins were extracted and then separated by sodium dodecyl sulfate (SDS) polyacrylamide gel electrophoresis (PAGE). Subsequently, the proteins were transferred to a nitrocellulose membrane. The membrane was blocked to eliminate nonspecific adsorption. It was incubated with the corresponding primary antibodies, and then with horseradish peroxidase-conjugated secondary antibodies. Finally, detection was carried out using enhanced chemiluminescence reagents. The primary antibodies utilized include P65 (catalog no. 8242, CST), PP65 (catalog no. 3033, CST), HIF-1 α (catalog no. 228649, abcam), α -SMA (catalog no. 14395-1-AP, Proteintech), COL1A1 (catalog no. E8F4L, CST), CXCL1 (catalog no. 12335-1-AP, Proteintech), β -actin (catalog no. 20536-1-AP, Proteintech), and PHD2 (catalog no. 19886-1-AP, Proteintech).

The ubiquitination of HIF-1 α was detected via immunoprecipitation and Western blot (WB) experiments. Cells were collected, and cell lysates were prepared. The specific antibody HIF-1 α was added, and the HIF-1 α protein was obtained by using Protein A/G mixed agarose beads. Subsequently, the ubiquitination status can be detected by Western blot.

RT-qPCR

Using TRIzol reagent (Ambin, USA), total RNA was extracted from the cells. RNA concentration and quality were evaluated by NanoDrop 2000c (Thermo Scientific, USA). According to the manufacturer's protocol, 2 μ g RNA was reverse transcribed into cDNA using the Transcriptor first-strand cDNA synthesis kit (Roche, Germany). β -Actin was set as an internal control. According to the manufacturer's protocol, quantitative real-time PCR was performed using SYBR Green Master (ROX) (Roche, Germany) on the 7500Fast system. After the reaction was completed, the fold change in target gene expression was calculated using the $2^{-\Delta\Delta C_t}$ formula. The primers for IL-1b were as follows: forward, 5'-GTGTCTTTCCCGTGGACCTT-3'; reverse, 5'-AATGGGAACGTCACACACCA-3'. Those for tumor necrosis factor (TNF)- α were as follows: forward, 5'-CGGGCAGGTCTACTTTGGAG-3'; reverse, 5'-ACCCTGAGCCATAATCCCCT-3'. Those for IL-6 were as follows: forward, 5'-CTTCTTGGGACTGATGCTGGT-3'; reverse, 5'-ACCCTGAGCCATAATCCCCT-3'. The primers for HIF-1 α were as follows: forward, 5'-GGCAGCAACGACACAGAAAC-3'; reverse, 5'-TTTTCGTTGGTGAGGGGAG-3'. The primers for CXCL1 were as follows: forward, 5'-TTGCCTCAATCCTGCATCCC-3'; reverse, 5'-GTTGGATTTGTCAGTTCAGCAT-3'. The primers for P65 were as follows: forward, 5'-AAGAAGAGTCCTTTCAGCGGACC-3'; reverse, 5'-TGCGGGAAGGCACAGCAAT-3'. The primers for β -actin were as follows: forward, 5'-TTCTGGGCATGGAGTCCT-3'; reverse, 5'-AGGAGGAGCAATGATCTTGATC-3'. The primers for PHD2 were as follows: forward, 5'-GCAGCATGGACGACCTGATA-3'; reverse, 5'-AGCAACCATGGCTTTCGTCC-3'.

Detection of mitochondrial membrane potential

The Mitochondrial Membrane Potential Detection Kit (including Mitochondrial Tracker Red) was purchased from Beyotime Biotechnology. Cells were treated according to the manufacturer's instructions to label the mitochondrial membrane potential, and image acquisition was carried out using a confocal microscope.

ECAR detection

The extracellular acidification rate curve (ECAR) was detected using an Agilent Seahorse XFp extracellular flux analyzer (Seahorse Bioscience). The experiment was carried out according to the manufacturer's instructions. The Agilent Seahorse XF glycolysis stress test kit (Agilent Technologies) was used to measure ECAR.

ELISA detection of CXCL1

The human CXC chemokine ligand 1 (CXCL1) enzyme-linked immunosorbent assay (ELISA) detection kit (CB12885-Hu) was purchased from Shanghai COIBO bio and detected according to the instructions provided by the reagent supplier.

Single-cell RNA sequencing and data analysis

Single-cell RNA sequencing was conducted by Shanghai Ouyi Biomedical Technology Co., Ltd. (Shanghai, China) according to standard protocols. The suspension of single cells was quality checked, with a concentration of 1250/ μ l and a cell viability rate of over 91%. The 10x Genomics platform utilized microfluidic technology to encapsulate cells and beads with cell barcodes in droplets. The droplets containing cells were collected, and the cells were lysed within the droplets, allowing the mRNA in the cells to bind to the cell barcodes on the beads, forming single-cell gel beads-in-emulsion (GEMs). Reverse-transcription reactions and cDNA library construction were performed within the droplets. The sample index on the library sequence was used to differentiate the source of the target sequences. The raw data generated from high-throughput sequencing were in fastq format. The official 10x Genomics software, Cell Ranger [<https://support.10xgenomics.com/single-cell-gene-expression/software/pipelines/latest/what-is-cell-ranger>], was used to perform data quality control and alignment to the reference genome. This software quantifies high-throughput single-cell transcriptomes by identifying the barcode sequences that distinguish cells and the unique molecular identifier (UMI) tags for different mRNA molecules within each cell, providing quality control statistics such as the number of high-quality cells, median gene expression, and sequencing saturation. The data were further quality controlled and processed using the Seurat package [26] on the basis of the initial quality control results from Cell Ranger. The FindAllMarkers function in the Seurat package was used to identify marker genes, which are genes that are differentially upregulated in each cell type compared with other cell types. Visualization of the identified marker genes was performed using the VlnPlot and FeaturePlot functions. The SingleR package was used to calculate the correlation between the expression profiles of the cells to be identified and reference datasets on the basis of the quantified single-cell reference expression data, assigning the cell type with the highest correlation in the reference dataset to the cells being identified, thereby reducing interference from subjective factors. For SECNIC analysis, GENIE3 and GRNBoost were used to infer co-expression regulatory networks. Using TF+ targets gene sets, each regulon of every cell was scored using AUCell, resulting in a binary matrix predicting cell activity. For pseudotemporal analysis, on the basis of the differentiation process of cells, cells were sorted using monocle to maximize transcriptional similarity. The algorithm presents the expression profile of each cell as a point in high-dimensional Euclidean space, with each gene having a dimension. Dimensionality reduction was performed using independent component analysis (ICA), and a minimum spanning tree (MST) was constructed on the cells. A specific algorithm was then used to find the longest path through the MST, corresponding to the longest sorting of cells with transcriptional similarity. This sorting generated a differentiation “trajectory” for each cell. Weighted gene co-expression network analysis (WGCNA) was carried out on the basis of the genetic system biology approach to gene expression, whereby genetic regulatory molecules related to complex

traits can be identified. Single-cell data from AP mice were used to detect co-expression gene networks in each cell type, and several gene modules were annotated according to cell subtypes. The cell subtypes corresponding to the module genes and their functions were determined.

Statistics

Count data are expressed as mean \pm standard deviation (SD). For comparisons between two groups, Student's *t*-test was used, and for comparison among more than three groups, one-way analysis of variance (ANOVA) was used. $P < 0.05$ was considered statistically significant and is indicated by an asterisk. $P < 0.01$ and $P < 0.001$ are indicated by two and three asterisks, respectively.

Results

The elimination of neutrophils and NETs can significantly improve acute pancreatitis

In this study, a large number of neutrophils and neutrophil extracellular traps (NETs, Fig. 1A, B) were found in acute pancreatitis tissues. To confirm their impact on AP, we treated AP mice with neutrophil neutralizing antibody (anti-LY6G) and NET inhibitor DNaseI, respectively. The study found that anti-LY6G and DNaseI downregulated neutrophils and NETs by 23% and 11%, respectively (Fig. 1C, D). Pathological tissue sections showed that reducing neutrophil infiltration and NETs accumulation can significantly improve the edema and inflammation of AP (Fig. 1E). Serum amylase and serum lipase were significantly downregulated in the anti-LY6G and DNaseI groups (Fig. 1F). Immunohistochemistry confirmed that the expressions of IL-1 β and IFN- γ in the anti-LY6G group and the DNaseI group were significantly reduced compared with the AP group (Fig. 1G, H).

scRNA-seq indicates that neutrophils in pancreatic tissue show heterogeneity during AP

This analysis completed single-cell transcriptome sequencing of pancreatic tissues in the control group and the AP group, with one sample in each group. The number of high-quality cells quantified by Cell Ranger in each sample ranged from 12,564 to 12,862. After quality control, 10,840 cells were obtained. The average number of UMIs in each cell ranged from 4733 to 8750, the average number of genes in each cell ranged from 445 to 2252, and the average proportion of mitochondrial genes in each cell ranged from 0.0050 to 0.0639. The number of genes detected in each cell, the UMI value, and the percentage of mitochondrial genes were all within the normal range. Subsequently, cluster analysis was performed on the gene expression data. A total of 15 different cell types were revealed. Each cell type was annotated on the basis of marker genes (Fig. 2A), and the atlas was visualized by T-distributed stochastic neighbor embedding (T-SNE) (Fig. 2B). The analysis results showed that there was a large amount of immune cell infiltration in AP pancreatic tissue, mainly macrophages and neutrophils. In recent years, people have paid more attention to macrophages and less research has been done on neutrophils. In view of this, we focus on neutrophils in AP.

We further clustered neutrophils. According to marker genes, cluster 1 subgroup was named Siglec-F + neutrophils, cluster 2 subgroup was named CD177 + neutrophils, and cluster 3 subgroup was named CD54 + neutrophils subgroup (Fig. 2 C, D). Research has

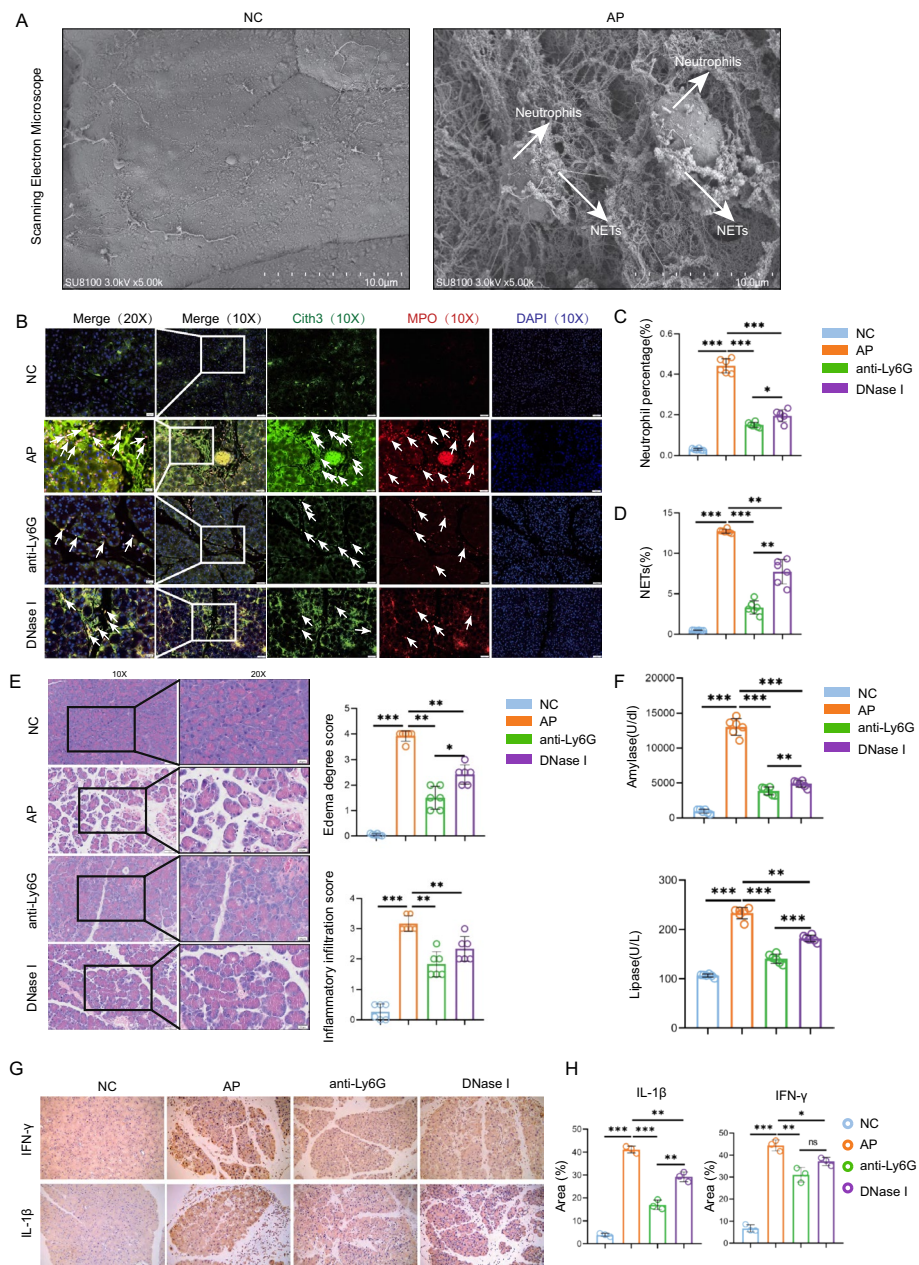


Fig. 1 Elimination of neutrophils and NETs can significantly improve acute pancreatitis **A** Scanning electron microscope images of pancreatic tissues in normal control group and AP group. The AP group contains neutrophils and NETs. **B** Fluorescence photo of neutrophil infiltration and NETs accumulation after treating the AP mouse model with neutrophil neutralizing antibody (anti-LY6G) and NETs inhibitor DNase I. **C** The proportion of neutrophils in each field of view of each group. **D** The proportion of NETs in each field of view of each group (MPO is red, representing neutrophils, pointed to by white arrows; CITH3 is bright green, pointed to by white arrows; yellow represents NETs, pointed to by white arrows). **E** H&E staining of each group and inflammation score and edema degree score. **F** Levels of serum amylase and lipase in mice of each group. **G** Immunohistochemical staining and expression statistics of IL-1 β and IFN- γ in each group. Student's *t*-test was used for comparison between two groups. **P* < 0.05 is considered statistically significant, ***P* < 0.01, ****P* < 0.001

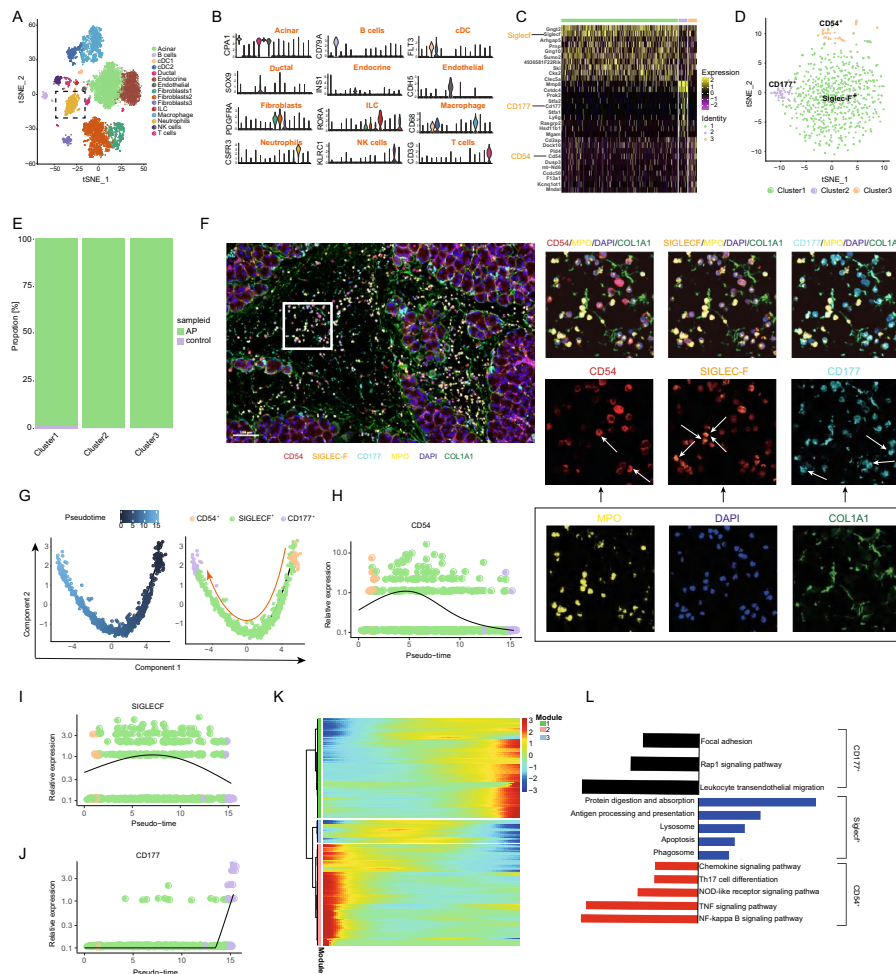


Fig. 2 scRNA-seq indicates that neutrophils in pancreatic tissue show heterogeneity during AP. **A** Cell atlas of pancreatic tissues of mice in normal control group and AP group. **B** Marker genes that distinguish various types of cells. **C** Heat map of marker gene expression of neutrophil subgroups. **D** Cell atlas of neutrophil subgroups. **E** Proportion of neutrophil subgroups in normal control group and AP group. **F** Multicolor immunofluorescence confirmed the existence of CD177 + neutrophil subgroup, CD54 + neutrophil subgroup, Siglec-F + neutrophil subgroup, neutrophils (MPO, yellow), CD177 is light blue, CD54 is red, Siglec-F is orange, and the nucleus is dark blue in pancreatic tissues of mice with AP. **G** Pseudotemporal analysis diagram of three neutrophil subgroups. **H–J** Expression trends of markers of three neutrophil subgroups on the time axis. **K** Gene dynamics analysis of neutrophils. The results show that there are three expression patterns of highly variable genes in neutrophils. **L** Kyoto Encyclopedia of Genes and Genomes (KEGG) enrichment analysis of highly variable genes in each module. Student's *t*-test was used for comparison between two groups. **P* < 0.05 is considered statistically significant, ***P* < 0.01, ****P* < 0.001

shown that Siglec-F is typically expressed in eosinophils. To verify which type of cells the Siglec-F + cells are, we evaluated the expression of eosinophil marker genes *Prg2*, *Prg3*, *Epx*, *Ear1*, *Ear2*, and *Ear6* in this subset [27, 28]. We found that these marker genes representing eosinophils were not expressed in these three subsets, while neutrophil marker genes such as *CSF3R*, *CXCR2*, *IL1R2*, *s100a8*, and *s100a* were expressed in all three subsets (Supplementary Fig. 1A, B). Therefore, it is a type of neutrophils that express Siglec-F. Figure 2E shows the proportion of each subgroup in AP. Multiple

immunohistochemistry techniques further confirmed the existence of three neutrophil subgroups in AP. We found that CD54+ neutrophils and Siglec-F+ neutrophils were mostly concentrated in the pancreatic interstitium, while CD177+ neutrophils were mostly concentrated in the pancreatic parenchyma (Fig. 2F). Pseudotemporal analysis indicated that CD177+ neutrophils were transformed from CD54+ neutrophils and Siglec-F+ neutrophils in turn (Fig. 2G). This indicates that, with the continuous infiltration of early CD54+ neutrophils and Siglec-F+ neutrophils, they then reach the pancreatic parenchyma and then differentiate into CD177+ neutrophils. CD177+ neutrophils highly express LY6G (Fig. 2C), which is a sign of neutrophil maturity. Figure 2H–J shows the expression trends of the three subgroup markers on the time axis. The expression of CD54 gradually decreased, indicating that the number of CD54+ neutrophils gradually decreased. The expression of Siglec-F first increased slowly and then decreased slowly, indicating that Siglec-F+ neutrophils are a cell in an excessive state, first increasing continuously and then decreasing continuously. The expression of CD177 was always low, but it suddenly increased when CD54 and Siglec-F returned to the baseline level. This indicates that CD177 is transiently expressed after neutrophil maturity. The results of gene dynamics showed that there were three expression patterns of highly variable genes in neutrophils (Fig. 2K): Pattern 1, where the gene expression gradually increased, which corresponded to CD177+ neutrophils; pattern 2, where the gene expression first increased and then decreased, which corresponded to Siglec-F+ neutrophils; and pattern 3, where the gene expression gradually decreased, which corresponded to CD54+ neutrophils. This indicates that the process of highly variable gene changes is the process of neutrophil subgroup differentiation. Module 1 corresponded to CD177+ neutrophils, and highly variable genes were enriched in focal adhesion, Rap1 signaling pathway, and leukocyte transendothelial migration pathway (Fig. 2L); module 2 corresponded to Siglec-F+ neutrophils, and highly variable genes were enriched in protein digestion and absorption, antigen processing and presentation, lysosome, apoptosis, phagosome pathway; module 3 corresponded to CD54+ neutrophils, and highly variable genes were enriched in chemokine signaling pathway, Th17 cell differentiation, nucleotide oligomerization domain (NOD)-like receptor signaling pathway, TNF signaling pathway, and NF- κ B signaling pathway. An important factor driving gene changes is transcription factors. We found that the change trend of the motif AUC value of transcription factors was consistent with the expression pattern of highly variable genes. In CD54+ neutrophils, the motif AUC values of ETS and JUN continuously decreased; in Siglec-F+ neutrophils, the motif AUC values of ETV6 and ETS2 first increased and then decreased; in CD177+ neutrophils, the motif AUC values of FOSL1 and NFE2 gradually increased (Supplementary Fig. 2A).

In acute pancreatitis, the infiltration of neutrophils is related to the activation of fibroblasts.

First, we characterized the fibroblast atlas in AP. The research results showed that there are three types of fibroblasts in AP. According to the expression of activation markers α -SMA (also known as ACTA2) and COL1A1 [29–31] (Fig. 3A). Fibroblasts 1 is named activated fibroblasts, namely myofibroblasts (Fig. 3B). For cluster 2, we found interesting results. Fibroblasts 2 exists in both the AP group and the control group (Fig. 3C). The

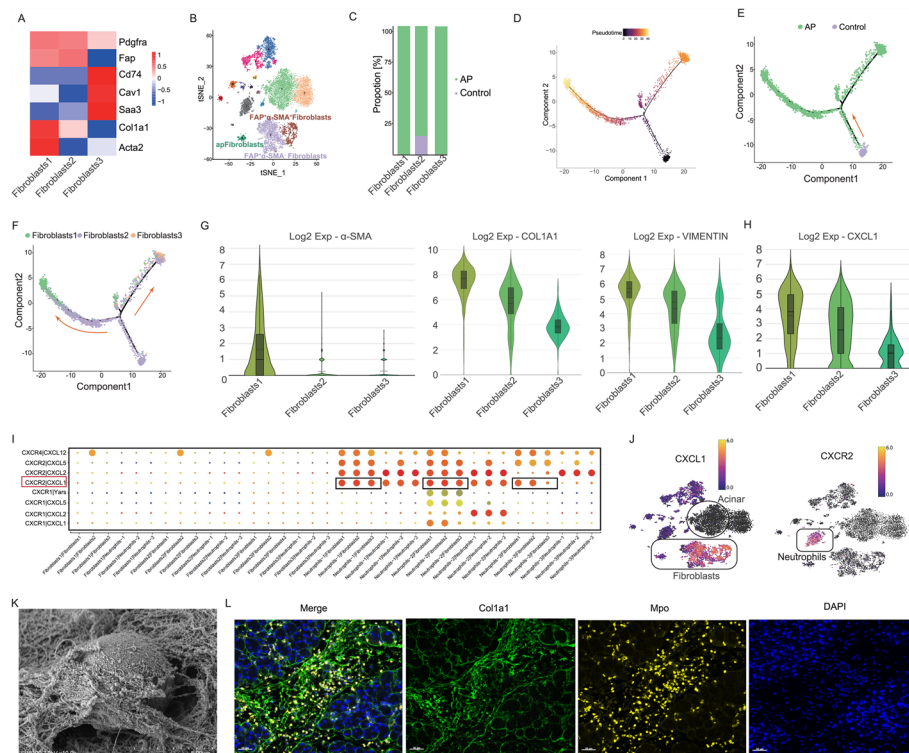


Fig. 3 The infiltration of neutrophils in acute pancreatitis is related to the activation of fibroblasts. **A** Heat map of marker expression of fibroblast subgroups. **B** T-SNE diagram of fibroblast subgroups. **C** Proportion diagram of fibroblast subgroups in normal control group and AP group. Pseudotemporal analysis diagram of fibroblast subgroups: **D** the pseudo-temporal direction diagram, with colors from deep to light, **E** the intergroup pseudotemporal diagram where fibroblasts differentiate from the control group to the AP group, and **F** the fibroblast subgroup differentiation diagram. **G** Relative expression levels of activation markers α -SMA, COL1A1, and VIMENTIN in each subgroup. **H** Relative expression level of CXCL1 in each subgroup. **I** Intercellular communication analysis: ligand–receptor pair. **J** CXCL1 is expressed in fibroblasts, and CXCR2 is expressed in neutrophils. **K** Scanning electron microscope image of neutrophils in interstitial fibers. **L** Immunofluorescence image, neutrophils (MPO, yellow), fibroblasts (COL1A1, green), nucleus (DAPI, blue). Student's *t*-test was used for comparison between two groups. **P* < 0.05 is considered statistically significant, ***P* < 0.01, ****P* < 0.001

difference is that fibroblasts 2 in AP highly expresses the activation marker COL1A1, while fibroblasts 2 cells in the control group do not express ACTA2 and COL1A1 (Fig. 3A). Therefore, strictly speaking, fibroblasts 2 in AP is a transitional fibroblast, and fibroblasts 2 in the control group is a quiescent fibroblast. This is reflected in Supplementary Fig. 2B. The results showed that fibroblasts 2 in the AP group highly expressed chemokines such as CXCL1, CXCL2, CCL2, and CCL7 compared with the NC group. Fibroblasts 3 specifically highly expresses CD74, CAV1, and SAA3 antigen-presenting cell markers (Fig. 3A), so it is named antigen-presenting fibroblasts (antigen-presenting fibroblasts, apFBs) (Fig. 3B). The results of pseudotemporal analysis showed that cluster 2 differentiated in two directions in acute pancreatitis and transformed into myofibroblasts and apFBs, respectively (Fig. 3D–F). Further analysis showed that, in the activation process of fibroblasts, the expression trend of CXCL1 was consistent with that of activation markers α -SMA, COL1A1, and VIMENTIN (Fig. 3G, H). Intercellular communication analysis showed that fibroblasts and neutrophils crosstalk with each other

through the CXCL1–CXCR2 ligand–receptor pair (Fig. 3I). In the T-SNE diagram, we found that fibroblasts highly expressed CXCL1 and neutrophils highly expressed CXCR2 (Fig. 3J). Previous studies have shown that pancreatic acinar cells express CXCL1 during acute pancreatitis. However, our results indicate that there is no expression of CXCL1 in acinar cells. This is because the single-cell data analysis reveals that only the acinar cells in the normal control group are enriched, while the acinar cells in the inflammatory group are necrotic and inactivated, thus not being enriched (Supplementary Fig. 3A). CXCL1 is scarcely expressed in the normal group, but is significantly highly expressed in the cerulein-stimulated group (Supplementary Fig. 3B). Given that CXCL1 is the natural ligand of CXCR2, we speculate that neutrophils may be chemotaxed to the pancreatic interstitium by CXCL1 secreted by fibroblasts. We confirmed by scanning electron microscopy and immunofluorescence that there are a large number of neutrophils in the pancreatic interstitial fibers (Fig. 3K, L).

The activation of fibroblasts depends on the NF- κ B signaling pathway induced by hypoxia

We explored the module genes unique to each fibroblast subgroup through WGCNA to characterize their functional characteristics. The results showed that the dataset was clustered into three modules (Fig. 4A). The clustering results showed that the brown module had the strongest correlation with fibroblasts 1 ($r=0.83$) (Fig. 4A). KEGG enrichment showed that the genes in this module were enriched in NF- κ B signaling pathway, phagosome, Hippo signaling pathway, tight junction, spliceosome, apoptosis, and ECM-receptor interaction pathway (Fig. 4B); the blue module had the strongest correlation with fibroblasts 2 ($r=0.64$) (Fig. 4A). KEGG enrichment showed that the genes in this module were enriched in AGE-RAGE signaling pathway in diabetic complications, TNF signaling pathway, PI3K-Akt signaling pathway, pathways in cancer, ferroptosis, NF- κ B signaling pathway, and JAK-STAT signaling pathway (Fig. 4C); the yellow module had the strongest correlation with fibroblasts 3 ($r=0.51$) (Fig. 4A). KEGG enrichment showed that the genes in this module were enriched in oxidative phosphorylation, IL-17 signaling pathway, antigen processing and presentation, C-type lectin receptor signaling pathway, MAPK signaling pathway, Toll-like receptor signaling pathway, and Th17 cell differentiation (Supplementary Fig. 2C). Most pancreatic fibroblasts originate from activated pancreatic stellate cells (PSCs) [32]. Therefore, we used PSCs to study the process of differentiation of resting fibroblasts (RFs) into activated fibroblasts (AFs). We found that, except for fibroblasts 3, the NF- κ B signaling pathway of fibroblasts 1 and fibroblasts 2 was activated. This is consistent with the expression distribution of activation markers and CXCL1 (Fig. 3G, H). For the differentiation process of fibroblasts, we performed pseudotemporal analysis on the expression of key genes. We found that, in fibroblasts 1 and fibroblasts 2, the NF- κ B signal was activated and the expression of HIF1- α continuously increased (Fig. 4D). Therefore, we speculate that this may be related to fibroblast activation and CXCL1 secretion.

We treated human pancreatic stellate cells with hypoxia for different lengths of time. We found that, as the hypoxia time prolonged, the expression of HIF-1 α gradually increased, and P65 and pP65 were continuously activated (Fig. 4E). The expression of the activation marker α -SMA gradually increased (Fig. 4F). Further immunofluorescence confirmed that hypoxia led to changes in cell morphology and upregulation of

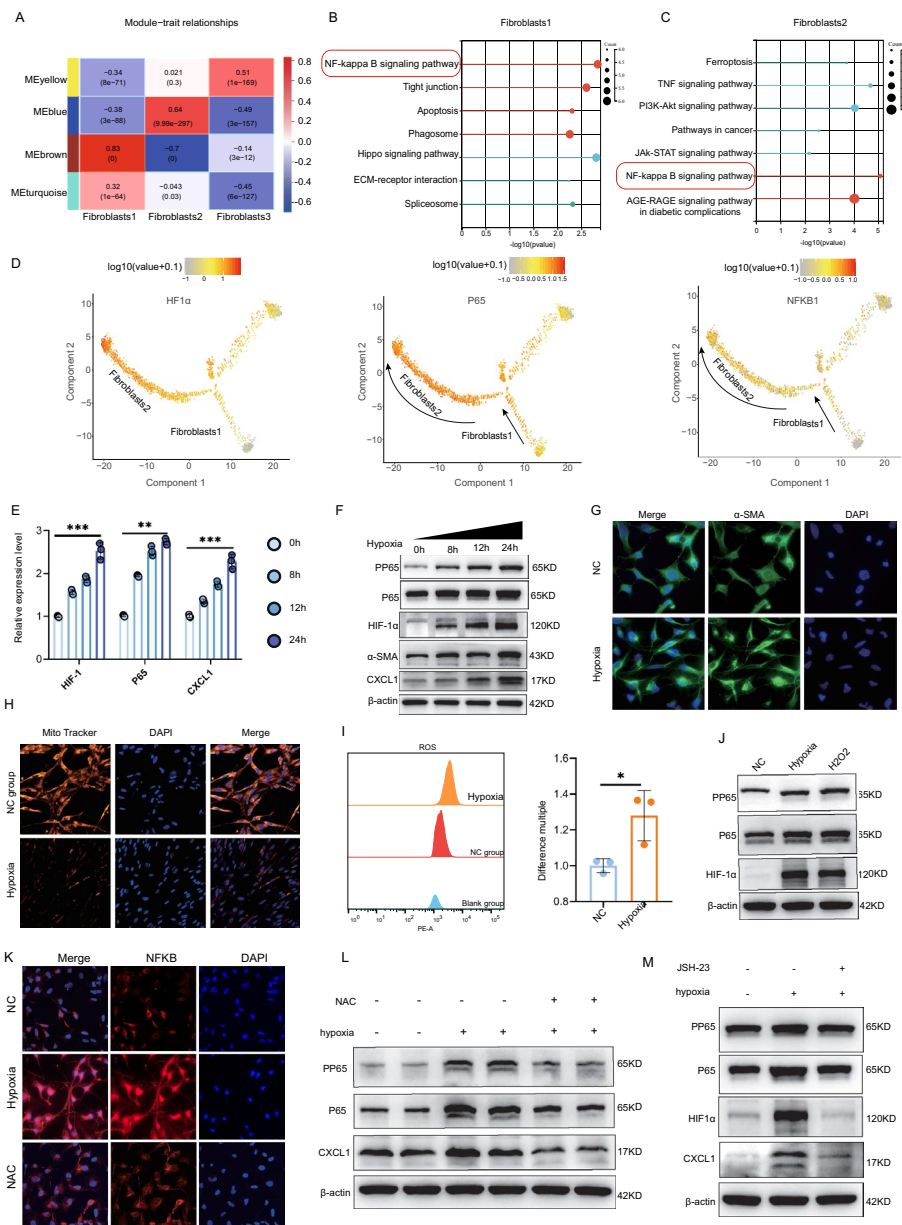


Fig. 4 The activation of fibroblasts depends on the NF- κ B signaling pathway induced by hypoxia. **A** Module-phenotype correlation diagram in WGCNA. **B** KEGG enrichment diagram of module genes corresponding to fibroblasts 1. **C** KEGG enrichment diagram of module genes corresponding to fibroblasts 2. **D** Relative expression levels of HIF-1 α , P65, and NF- κ B1 during the differentiation process in each subgroup. **E** Expression levels of HIF-1 α , P65, and CXCL1 at the transcriptional level as hypoxia time prolongs. **F** Western blot diagrams of NF- κ B signaling molecules, HIF-1 α , activation marker α -SMA, and CXCL1 as hypoxia time prolongs. **G** Fluorescence images of α -SMA in each group. **H** Fluorescence images of mitochondrial membrane potential in each group. **I** Flow cytometry diagrams of ROS in each group. **J** Western blot diagrams of NF- κ B signaling molecules and HIF-1 α under hydrogen peroxide stimulation. **K** Expression of pP65 in the nucleus of PSCs after hypoxia and NAC treatment. **L** Western blot diagrams of NF- κ B signaling molecules and CXCL1 after hypoxia and NAC treatment. **M** Western blot diagrams of NF- κ B signaling molecules, HIF-1 α , and CXCL1 after JSH-23 treatment of PSCs. Student's *t*-test was used for comparison between two groups, and one-way ANOVA was used for comparison among more than three groups. **P* < 0.05 is considered statistically significant, ***P* < 0.01, ****P* < 0.001

α -SMA (Fig. 4G). The above proves that hypoxia can activate the HIF-1 α -NF- κ B signal and promote fibroblast activation. In addition, we found that fibroblasts can be activated by acinar cells stimulated with cerulein and participate in the inflammatory response (Supplementary Fig. 1C). The experimental results show that, under both normal and hypoxic conditions, PSC cells in the cerulein group significantly highly express α -SMA, COL1A1, and CXCL1, and hypoxia further increases their expression (Supplementary Material 1D). The expression trends of the inflammatory factors IL-1 β , TNF- α , and IL-6 in the acinar cells in the lower chamber are consistent with the activation trend of PSC (Supplementary Fig. 1E). Hypoxia can cause a decrease in mitochondrial membrane potential and an increase in ROS (Fig. 4H, I), which is consistent with previous studies. We guess that the increase in ROS caused by hypoxia may be the initiating factor for activating NF- κ B and PSCs. To confirm this guess, we treated with H₂O₂. The results showed that the results of H₂O₂ treatment were consistent with those of hypoxia treatment. Compared with the control group, hypoxia and hydrogen peroxide led to HIF-1 α accumulation and NF- κ B signal activation (Fig. 4J). In addition, we also found that hypoxia and H₂O₂ treatment both promoted the nuclear translocation of P65 (Fig. 4K). NAC elimination of ROS can significantly reverse NF- κ B activation and CXCL1 secretion caused by hypoxia (Fig. 4L). Further inhibition of the NF- κ B signal significantly reduced the accumulation of HIF-1 α and the secretion of CXCL1 (Fig. 4M).

NF- κ B promotes HIF-1 α accumulation by inhibiting PHD2, thereby enhancing PSC activation and CXCL1 secretion

To verify that, under hypoxia, the activation of fibroblasts and the expression of CXCL1 depend on the NF- κ B-HIF-1 α -signal, we conducted the following experiments: We transfected si-p65 into PSCs and observed the mRNA and protein expression of HIF-1 α . First, we verified that the knockout efficiency of P65 was as expected (Fig. 5A, B). Further, it was found that knockdown of P65 could significantly reverse the increase in HIF-1 α transcription and protein expression induced by hypoxia (Fig. 5C, D). This indicates that NF- κ B promotes the expression of HIF-1 α in PSCs. Immunofluorescence clearly showed that knockdown of P65 significantly reduced the nuclear expression of HIF-1 α (Fig. 5E). We confirmed that the knockdown efficiency of si-HIF-1 α was significantly different (Fig. 5F, G). Further experimental results showed that knocking down HIF-1 α could significantly inhibit the expression of α -smooth muscle actin (α -SMA) and CXCL1 (Fig. 5H-I), indicating that HIF-1 α is necessary for the activation of pancreatic stellate cells. Under hypoxic conditions, we transfected pancreatic stellate cells with si-NF- κ B, si-HIF-1 α , and si-NF- κ B + si-HIF-1 α , respectively, and then measured the expression level of CXCL1. Compared with the normoxic state, knocking out either NF- κ B or HIF-1 α alone cannot counteract the increase in CXCL1 expression caused by hypoxia. However, simultaneously knocking down NF- κ B and HIF-1 α can further reduce the expression of CXCL1, indicating that NF- κ B and HIF-1 α act synergistically to promote CXCL1 expression (Supplementary Fig. 1F).

Studies have shown that, under normal oxygen partial pressure, HIF-1 α protein will be rapidly degraded and maintained at a low level. However, when cells are in a hypoxic environment, ubiquitination degradation is inhibited, leading to its accumulation in cells [33]. We used MG-132 to inhibit the ubiquitin-proteasome system and observed the

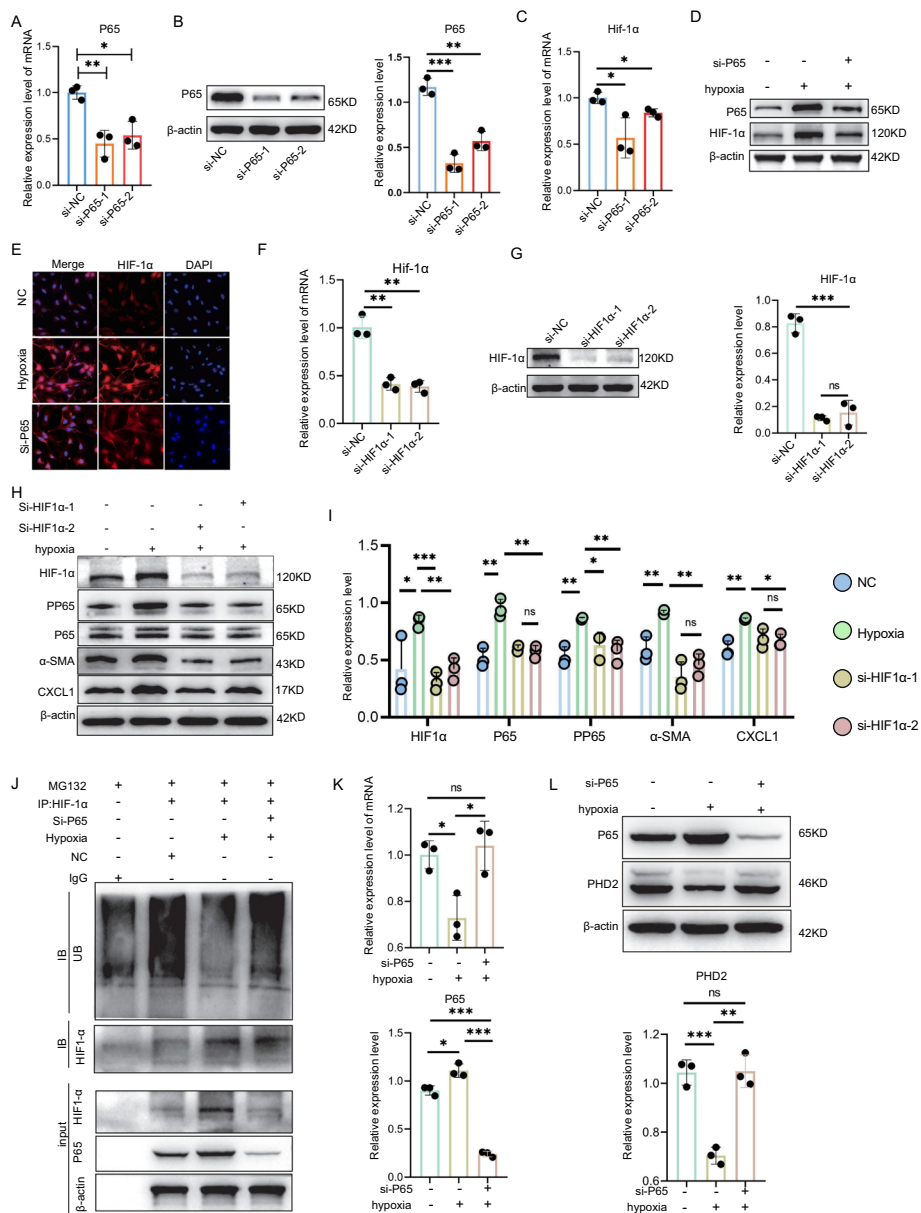


Fig. 5 NF-κB promotes HIF-1α accumulation by inhibiting PHD2, thereby enhancing PSC activation and CXCL1 secretion. **A** Verification of the expression level of P65 mRNA after PSCs are transfected with si-P65. **B** Verification of the protein expression level of P65 after PSCs are transfected with si-P65. **C** Observation of the mRNA level of HIF-1α after PSCs are transfected with si-P65. **D** Western blot diagram of P65 and HIF-1α after PSCs are transfected with si-P65. **E** Expression level of HIF-1α in the nucleus after PSCs are transfected with si-P65. **F** Verification of the expression level of HIF-1α mRNA after PSCs are transfected with si-HIF-1α. **G** Verification of the protein expression level of HIF-1α after PSCs are transfected with si-HIF-1α. **H–I** Western blot diagram of NF-κB signaling molecules, α-SMA, and CXCL1 after PSCs are transfected with si-HIF-1α. **J** MG-132 inhibits the ubiquitin–proteasome system, as shown by the effect of si-P65 on HIF-1α ubiquitination. An IP experiment was performed on HIF-1α to verify the ubiquitin level of each group by Western blot. The expression of P65 and HIF-1α in total protein was verified by a Western blot experiment. **K** mRNA expression level of PHD2 after PSCs are transfected with si-P65. **L** Western blot diagram of PHD2 after PSCs are transfected with HIF-1α. Student’s *t*-test was used for comparison between two groups. **P* < 0.05 is considered statistically significant, ***P* < 0.01, ****P* < 0.001

effect of si-P65 on HIF-1 α ubiquitination. We found that hypoxia could significantly reduce HIF-1 α ubiquitination, while knockout of P65 would increase HIF-1 α ubiquitination under hypoxic conditions (Fig. 5F). Studies have confirmed that, when the activity of PHD2 is reduced, the proline residue of HIF-1 α cannot be hydroxylated, so it cannot be recognized and bound by VHL, avoiding ubiquitination and proteasome degradation [34]. Therefore, we observed the effect of si-P65 on PHD2 under hypoxia. We found that knockdown of P65 could significantly increase the mRNA and protein expression of PHD2 (Fig. 5G, H). Therefore, in addition to directly promoting HIF-1 α transcription, P65 can also promote the protein accumulation of HIF-1 α by inhibiting PHD2. The above results indicate that NF- κ B not only acts synergistically with HIF-1 α to promote the transcription of CXCL1, but also enhances the stability of HIF-1 α by inhibiting PHD2 (Fig. 5F). This further strengthens the regulation of the chemokine CXCL1 by HIF-1 α . This may represent another pathway through which NF- κ B and HIF-1 α synergistically promote the expression of CXCL1.

The NF- κ B-HIF-1 α signal promotes neutrophil infiltration by promoting fibroblast secretion of CXCL1 through glycolysis

To explore the mechanism by which the NF- κ B-HIF-1 α signal promotes fibroblast activation and CXCL1 expression, we conducted a series of experiments. Previous results showed that HIF-1 α is necessary for PSC activation. Then, how HIF-1 α exerts its function needs to be clarified. Past studies have shown that the intracellular accumulation of HIF-1 α can enhance glycolysis, and an increase in glycolysis can promote the activation of hepatic stellate cells [35]. However, it is unknown whether glycolysis affects the activation of PSCs. We used 2-deoxyglucose (2-DG) to inhibit the glycolysis process of PSCs under hypoxic conditions. We found that 2-DG significantly reduced the activation markers COL1A1, α -SMA, and CXCL1 of PSCs (Fig. 6A, B). At the same time, we detected the mRNA of inflammatory factors. We found that inhibiting glycolysis could significantly downregulate the expressions of IL-6, IL-1 β , TNF- α , and CXCL1 (Fig. 6C). Immunofluorescence confirmed that inhibiting glycolysis could significantly downregulate α -SMA and KI67, indicating that inhibiting glycolysis can inhibit hypoxia-mediated PSCs activation and proliferation (Fig. 6D, E). We extracted neutrophils from the peripheral blood of patients with pancreatitis and co-cultured them with PSCs through Transwell co-culture chambers. We added and did not add 2-DG to the lower chamber and observed the number of neutrophils in the lower chamber. We found that inhibiting glycolysis can lead to a decrease in neutrophil chemotaxis in the lower chamber (Fig. 6F). Further, we confirmed the regulatory effect of the NF- κ B-HIF-1 α signal on glycolysis through si-P65 and overexpression (OE)-HIF-1 α . Knockout of P65 can significantly inhibit basal glycolytic capacity and maximum glycolytic capacity, and overexpression of HIF-1 α on this basis can enhance glycolysis (Fig. 6G–I). In addition, the protein levels of COL1A1, α -SMA, and CXCL1 and the mRNA levels of IL-6, IL-1 β , TNF- α , and CXCL1 all decreased with glycolysis inhibition and increased with glycolysis enhancement (Fig. 6J–L). We also found that si-P65 and OE-HIF-1 α can regulate the migration and proliferation of PSCs. si-P65 reduces migration and proliferation, and OE-HIF-1 α can reverse the effect of si-P65 (Fig. 6M, N). Finally, we detected the level of CXCL1

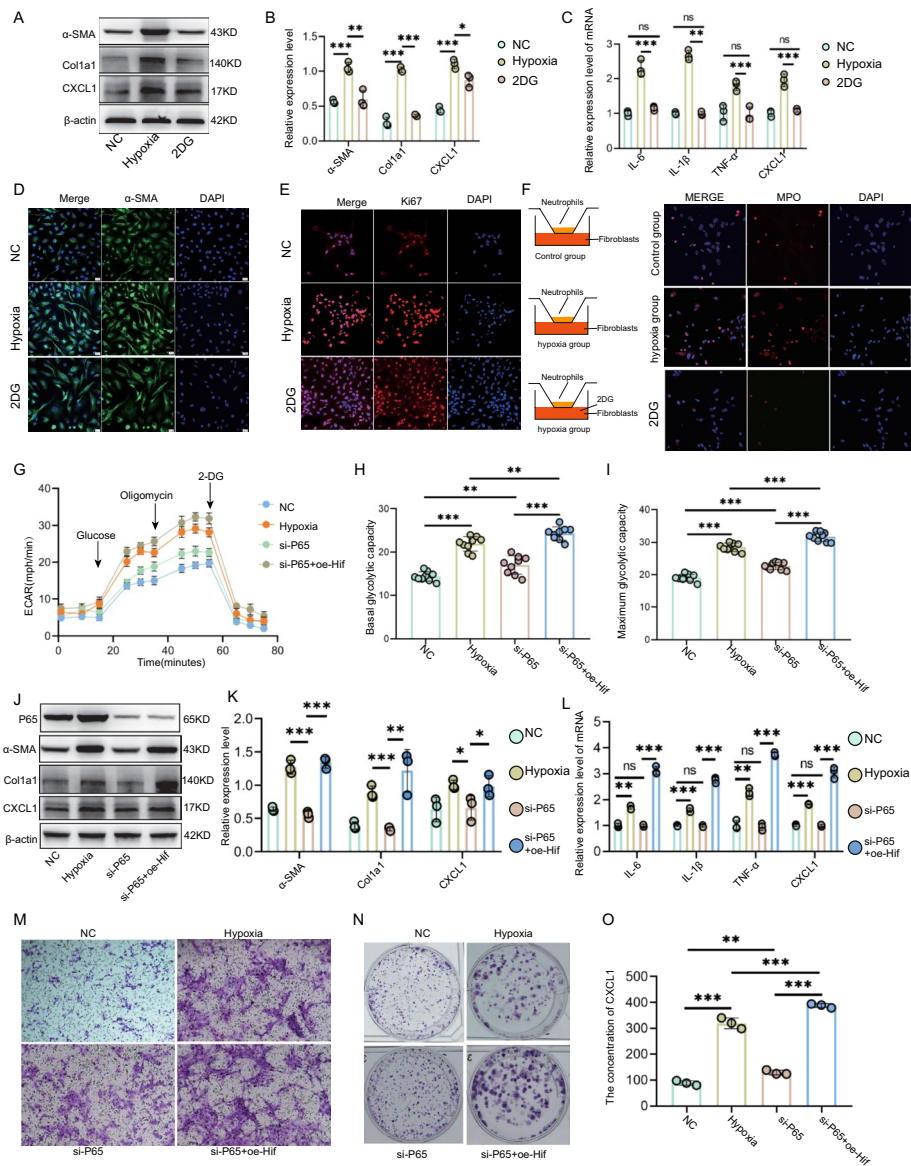


Fig. 6 The NF-κB-HIF-1α signal promotes neutrophil infiltration by promoting fibroblast secretion of CXCL1 through glycolysis. **A, B** Western blot diagrams of COL1A1, α-SMA, and CXCL1 after 2-DG treatment of PSCs. **C** mRNA levels of IL-6, IL-1β, TNF-α, and CXCL1 after 2-DG treatment of PSCs. **D** Fluorescence image of significantly reduced α-SMA after 2-DG treatment of PSCs. **E** Fluorescence image of significantly reduced ki-67 after 2-DG treatment of PSCs. **F** Transwell co-culture chamber: PSCs are cultured in the lower chamber with or without 2-DG added, neutrophils are cultured in the upper chamber, and the number of neutrophils in the lower chamber is observed after 24 h (neutrophils are labeled with MPO, green). **G** Effect of transfection of PSCs with si-P65 or OE-HIF-1α on extracellular acidification rate curve (ECAR). **H** Effect of transfection of PSCs with si-P65 and OE-HIF-1α on basal glycolytic capacity. **I** Effect of transfection of PSCs with si-P65 and OE-HIF-1α on maximum glycolytic capacity. **J, K** Protein levels of COL1A1, α-SMA, and CXCL1 after transfection of PSCs with si-P65 or OE-HIF-1α. **L** mRNA expression levels of IL-6, IL-1β, TNF-α, and CXCL1 after transfection of PSCs with si-P65 and OE-HIF-1α. **M** Migration images after transfection of PSCs with si-P65 and OE-HIF-1α. **N** Clone formation images after transfection of PSCs with si-P65 and OE-HIF-1α. **O** Secretion level of CXCL1 after transfection of PSCs with si-P65 and OE-HIF-1α. Student's *t*-test was used for comparison between two groups. **P* < 0.05 is considered statistically significant, ***P* < 0.01, ****P* < 0.001

secreted by the si-P65 and si-HIF-1 α + OE-HIF-1 α groups by ELISA. The results were consistent with expectations. si-P65 reduced the secretion of CXCL1, while OE-HIF-1 α increased its secretion (Fig. 6O).

Blocking the NF- κ B–HIF-1 α –CXCL1 signaling axis reduces neutrophil infiltration and improves AP

SC75741 intraperitoneal injection treatment was performed 3 h before the establishment of the acute pancreatitis model, and the model was established immediately after the last injection. SC75741 is a widely effective NF- κ B inhibitor. Through H&E staining, it was found that SC75741 significantly reduced pancreatic tissue edema and inflammation scores (Fig. 7A, B). WB results showed that SC75741 inhibited the increase of P65, PP65, and CXCL1 in AP mice (Fig. 7C). Immunohistochemistry further confirmed that SC75741 reduced the expression of CXCL1 in AP pancreatic tissue (Fig. 7D). At the same time, immunofluorescence confirmed that SC75741 treatment could reduce the accumulation of neutrophils and NETs (Fig. 7E), thereby improving AP. Further, we used PX-478 to inhibit the HIF-1 α signal (Fig. 7F), and used SRT3109 to antagonize CXCR2 (Fig. 7F), and then observed the progress of AP. Pathological tissue sections showed that PX-478 and SRT3109 significantly reduced pancreatic tissue edema and inflammation infiltration scores (Fig. 7G). Inhibiting HIF-1 α and antagonizing CXCR2 respectively can significantly reduce serum amylase and serum lipase (Fig. 7H). PX-478 and SRT3109 significantly reduced the mRNA of inflammatory factors IL-1 β , TNF- α , and IL-6 in AP pancreatic tissue (Fig. 7I). WB and immunohistochemistry showed that inhibiting NF- κ B could significantly reduce the expression of CXCL1 (Fig. 7J, K). Finally, we evaluated the effects of PX-478 and SRT3109 on neutrophil infiltration. We found that blocking NF- κ B and CXCR2 respectively could significantly reduce the accumulation of neutrophils and NETs (Fig. 7L). The above research results prove that blocking the NF- κ B–HIF-1 α –CXCL1 signal in vivo can reduce the accumulation of neutrophils and NETs and improve AP (Fig 8).

Discussion

Our study is the first to prove in AP that fibroblast activation is an immunological driving factor for neutrophil infiltration. This study elucidates that glycolysis driven by NF- κ B–HIF-1 α is the intrinsic molecular mechanism by which fibroblasts chemotactically attract neutrophils. In the early stage of pancreatitis, fibroblasts can be activated by acinar cells stimulated with cerulein and participate in the inflammatory response. This may be a key factor contributing to the aggravation of pancreatitis [33]. This study not only demonstrates the role of neutrophils in the development of acute pancreatitis but, more importantly, reveals the immunomodulatory role of fibroblasts in the early stage of acute inflammation.

Neutrophil recruitment is a rate-limiting step in pancreatic tissue and distant organ damage [36, 37]. In addition, neutrophils can exacerbate acute pancreatitis and systemic inflammation by releasing NETs [11, 38]. Therefore, inhibiting neutrophil infiltration and the release of NETs is crucial for reducing AP. We used single-cell transcriptome sequencing technology and found that there are three neutrophil subgroups in acute pancreatitis tissues. Pseudotemporal analysis suggests that they are

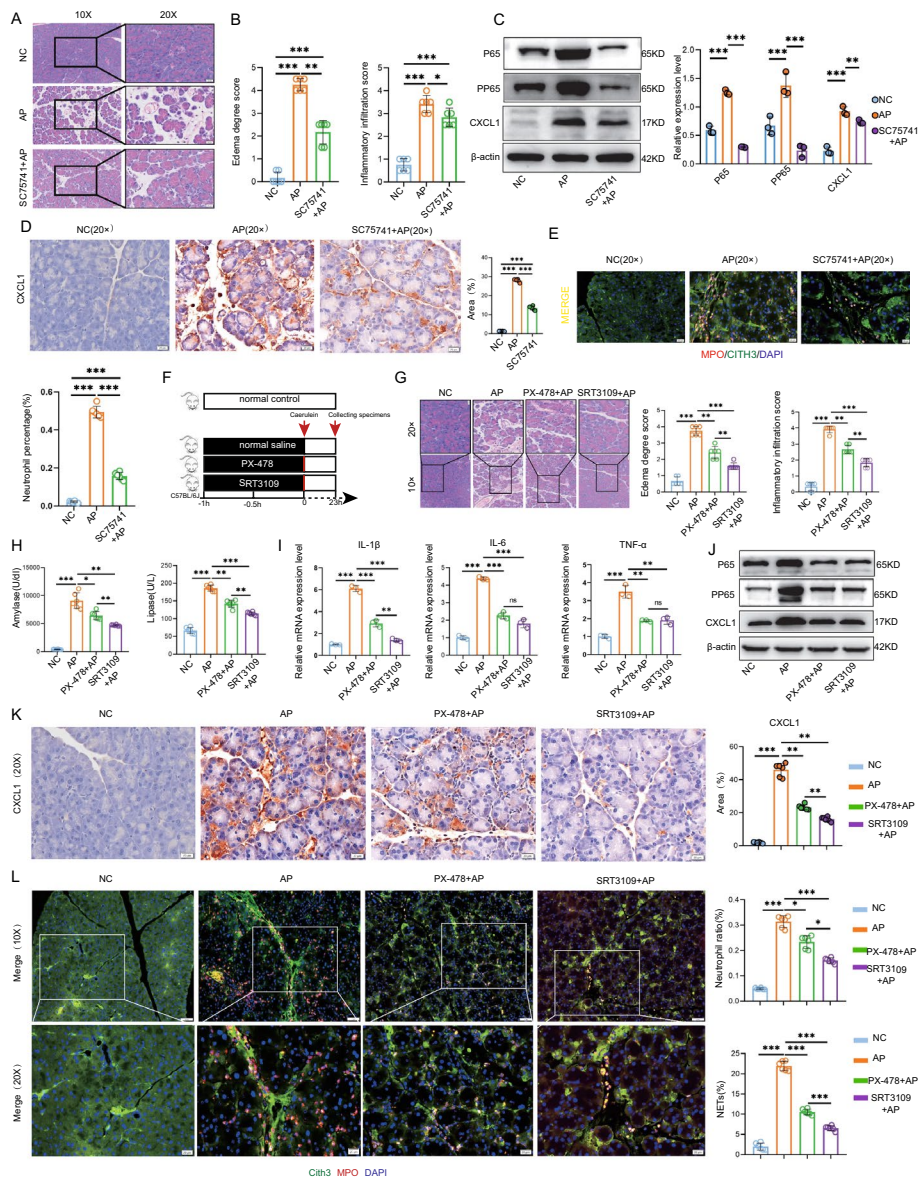


Fig. 7 Blocking the NF- κ B-HIF-1 α -CXCL1 signaling axis reduces neutrophil infiltration and improves AP. **A** H&E staining, edema degree score, and inflammation score of pancreatic tissues of mice in normal control group, AP group, and AP + SC75741 (NF- κ B inhibitor) group. **B** Western blot diagrams of P65, pP65, and CXCL1 in pancreatic tissues of normal control group, AP group, and SC75741 + AP group. **C** Immunohistochemical diagram of CXCL1 in pancreatic tissues of normal control group, AP group, and SC75741 + AP group. **D** Percentage of neutrophils and immunofluorescence diagram of NETs in pancreatic tissues of normal control group, AP group, and SC75741 + AP group (MPO, red, neutrophil marker; CITH3, green; yellow image is NETs). **E** Percentage of neutrophils and immunofluorescence diagram of NETs in pancreatic tissues of normal control group, AP group, and SC75741 + AP group (MPO, red, neutrophil marker; CITH3, green; yellow image is NETs). **F** Diagram showing animal experiment operation. **G** H&E staining, edema degree score, and inflammation score of pancreatic tissues of mice in normal control group, AP group, AP + PX-478 (HIF-1 α inhibitor) group, and AP + SRT3109 (CXCR2 antagonist) group. **H** Levels of serum amylase and lipase in mice in normal control group, AP group, AP + PX-478 (HIF-1 α inhibitor) group, and AP + SRT3109 (CXCR2 antagonist) group. **I** mRNA expression levels of inflammatory factors in each group. **J** Western blot diagrams of P65, pP65, and CXCL1 in each tissue. **K** Immunohistochemical diagrams of CXCL1 in each group. **L** Percentage of neutrophils and immunofluorescence diagram of NETs in pancreatic tissues of each group (MPO, red, neutrophil marker; CITH3, green; yellow image is NETs). Student's *t*-test was used for comparison between two groups. **P* < 0.05 is considered statistically significant, ***P* < 0.01, ****P* < 0.001

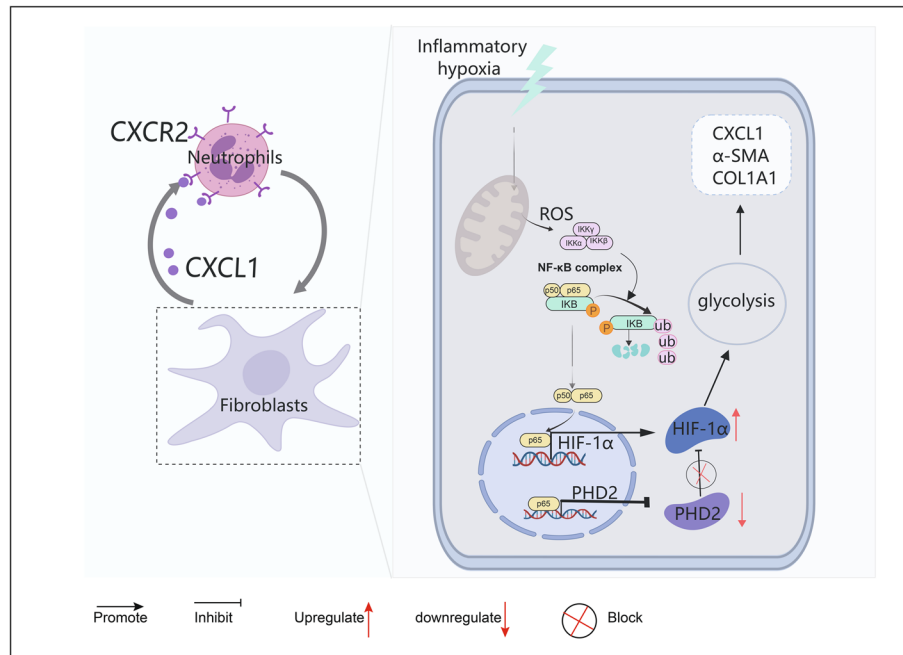


Fig. 8 Aseptic inflammation caused by acinar cell injury leads to local tissue hypoxia. The hypoxic environment causes a decrease in the mitochondrial membrane potential of pancreatic stellate cells and the release of reactive oxygen species. Reactive oxygen species activate the NF- κ B signaling pathway, and the nuclear entry of pP65 increases. On the one hand, pP65 directly binds to the promoter region of HIF-1 α to promote the expression of HIF-1 α . On the other hand, pP65 can inhibit the expression of PHD2, thereby blocking the ubiquitination and degradation of HIF-1 α by PHD2, ultimately leading to the accumulation of HIF-1 α in cells. HIF-1 α can promote glycolysis and lead to the activation of PSCs to release cytokines such as CXCL1, thereby chemotactically attracting the infiltration of neutrophils and aggravating AP

neutrophils at different maturation stages and have a linear relationship of sequential differentiation. In addition, the research group found through immunofluorescence that some of them are MPO-negative neutrophils. Under normal circumstances, normal neutrophils participate in immunoregulation through MPO. The presence of MPO-negative neutrophils may disrupt the immune balance. On the one hand, this may lead to a weakened immune response to certain pathogens, increasing the body's susceptibility and exacerbating pancreatitis and related complications. On the other hand, owing to the lack of MPO, they have a defect in the formation of NETs, which may reduce the tissue damage associated with NETs. Overall, the role of myeloperoxidase-negative neutrophils in the pathogenesis of pancreatitis is rather complex. They may exacerbate the inflammatory response and tissue damage through the release of inflammatory mediators and other means, but they may also exert a certain protective effect on the condition owing to abnormal NETs formation and other factors. The specific impacts still need to be further elucidated through more research.

Interestingly, they all highly express CXCR2, which means they are all chemotaxed by CXCR2 ligands. Xiong et al.'s research shows that overexpression of endothelial cell CD276 will lead to a significant upregulation of CXCL1 and promote neutrophil infiltration and the formation of NETs through the CXCL1–CXCR2 signal [39]. Our research shows that, in the early stage of AP, fibroblast proliferation and activation

occur, and a large amount of CXCL1 is secreted. Past studies have confirmed that fibroblasts in pancreatitis mainly originate from stellate cells [32, 40, 41]. Therefore, we chose PSCs to study the molecular mechanism of fibroblast activation and the release of CXCL1 in the process of AP. Current studies have identified several signaling pathways that activate PSCs [30, 42], mainly including MAPK signaling pathway, PI3K/AKT signaling pathway, JAK/STAT signaling pathway, NF- κ B signaling pathway, and TGF- β /SMAD related pathway [43–45]. Our research shows that glycolysis mediated by the NF- κ B–HIF-1 α signal in a hypoxic environment is an important signaling pathway for promoting the activation of PSCs. First, through pseudotemporal analysis, we found that, during the transformation of PSCs into activated fibroblasts, the NF- κ B signaling pathway is activated and HIF-1 α continuously increases. More precisely, the NF- κ B–HIF-1 α signal is activated in fibroblasts 1 and fibroblasts 2. The experimental results show that, with the increase of hypoxia time, the expressions of P65, pP65, and HIF-1 α gradually increase, and the expression of the activation marker SMA also gradually increases. Further research found that hypoxia leads to a decrease in mitochondrial membrane potential and an increase in ROS in PSCs. Studies have shown that intracellular ROS caused by mitochondrial dysfunction can activate the NF- κ B signal [46]. By treating PSCs with H₂O₂ in vitro, it was found that the NF- κ B signal is activated and the nuclear translocation of pP65 increases, and the secretion of CXCL1 increases. Antioxidants and NF- κ B inhibitors can significantly reduce the effect of H₂O₂ on PSCs. This indicates that the activation of PSCs and the secretion of CXCL1 depend on the hypoxia-induced ROS–NF- κ B signal. It is worth mentioning that acinar cells are another source of CXCL1 production (Supplementary Fig. 3B). However, owing to the limitations of single-cell sequencing technology, acinar cells producing CXCL1 have not been identified in the pancreatic tissues of AP, which may introduce certain biases to the research conclusions.

It is known that, in endothelial cells and epithelial cells, NF- κ B can directly bind to the HIF-1 α promoter and promote the mRNA expression of HIF-1 α [47, 48]. To verify whether NF- κ B in PSCs affects its activation by regulating HIF-1 α , we used siRNA to knockdown P65 in PSCs and found that the mRNA and protein levels of HIF-1 α were significantly downregulated, and at the same time SMA- α and CXCL1 were also significantly downregulated. This indicates that, in PSCs, NF- κ B affects its activation and the secretion of CXCL1 by regulating HIF-1 α transcription. In addition, this study also confirmed the previous research findings. Compared with the normoxic condition, knockdown of either NF- κ B or HIF-1 α alone cannot counteract the increase in CXCL1 caused by hypoxia. However, simultaneous knockdown of NF- κ B and HIF-1 α can further reduce the expression of CXCL1, indicating that NF- κ B and HIF-1 α act synergistically to promote the expression of CXCL1 (Supplementary Fig. 1F).

The accumulation of HIF-1 α in cells is regulated not only at the transcriptional level but also by posttranslational modifications. Past studies have shown that, under normal oxygen concentration, HIF-1 α will be hydroxylated by prolyl hydroxylase (PHD) at specific proline residues. The hydroxylated HIF-1 α can be recognized and bound by von Hippel–Lindau (VHL) protein, and then recruit ubiquitin ligase complexes to promote the ubiquitination and proteasome degradation of HIF-1 α [49]. Under hypoxic conditions, the activity of PHD2 is inhibited, and HIF-1 α cannot be hydroxylated, thus

avoiding ubiquitination and degradation and increasing the level of HIF-1 α [34]. It is worth mentioning that we found that knocking out P65 under hypoxic conditions led to an increase in the ubiquitination level of HIF-1 α . Further experiments proved that knocking out P65 could significantly upregulate the mRNA and protein expression levels of PHD2. Therefore, we conclude that P65 can affect both the transcriptional level of HIF-1 α and its protein ubiquitin degradation pathway. This could be another pathway through which NF- κ B and HIF-1 α exert a synergistic effect.

It is known that HIF-1 α -mediated glycolysis can promote the activation and inflammatory response of cardiac fibroblasts, tumor-associated fibroblasts, and hepatic stellate cells [50–52]. Next, we explored whether the activation of PSCs under hypoxic conditions depends on HIF-1 α -mediated glycolysis. As expected, the activation of PSCs and the expression of CXCL1 depend on glycolysis. Blocking glycolysis with 2-DG significantly inhibited the expression of activation markers and CXCL1. Immunofluorescence also confirmed the decreased expression of KI67 and SMA- α . Next, we confirmed the regulatory effect of the NF- κ B–HIF-1 α signal axis on glycolysis in PSC under hypoxic conditions. We co-transfected SI-P65 and OE-HIF-1 α . We found that, compared with the hypoxic control group, knocking out P65 significantly inhibited the glycolysis level, while the glycolysis level of the SI-P65 and OE-HIF-1 α co-transfection group was significantly enhanced. At the same time, we found that the proliferation and migration abilities of PSCs were consistent with the change level of glycolysis. Further, the secretion level of CXCL1 in each group was detected by ELISA, and the result was consistent with the change trend of glycolysis. Finally, we confirmed the potential role of this signaling pathway in improving AP by blocking each node of the NF- κ B–HIF-1 α –CXCL1 signaling axis *in vivo*, proving that this signaling pathway is a promising target for the treatment of AP.

Conclusions

This study demonstrated, for the first time, that the activation of fibroblasts is one of the immunological driving factors for neutrophil infiltration, and elucidated that glycolysis driven by NF- κ B–HIF-1 α is the intrinsic molecular mechanism by which fibroblasts secrete CXCL1 to chemotactically attract neutrophils. It is noteworthy that this study, through relevant experiments, has proven that acinar cells are also important source cells of CXCL1. However, owing to the limitations of single-cell sequencing technology, acinar cells producing CXCL1 have not been identified in the pancreatic tissue of AP. This technical bottleneck has, to a certain extent, affected the researchers' judgment on the contribution level of fibroblasts in driving neutrophil infiltration. Nevertheless, on the basis of the existing data, the signaling pathway related to the activation of fibroblasts driving neutrophil infiltration still provides a highly promising target for the treatment of AP.

Abbreviations

AP	Acute pancreatitis
SAP	Severe acute pancreatitis
ALI	Acute lung injury
ARDS	Acute respiratory distress syndrome
NETs	Neutrophil extracellular traps
UMI	Unique molecular identifier

SD Standard deviation
T-SNE T-distributed stochastic neighbor embedding
PHD Prolyl hydroxylase
VHL Von Hippel–Lindau protein

Supplementary Information

The online version contains supplementary material available at <https://doi.org/10.1186/s11658-025-00734-6>.

Supplementary file 1. Figure 1: (A) Neutrophil markers. (B) Eosinophil markers. (C) Schematic diagram of co-culture of mouse acinar cells (266-6) and mouse pancreatic stellate cells (PSC): Under hypoxic and nonhypoxic conditions, we used immortalized mouse pancreatic acinar cells (266-6) and mouse pancreatic stellate cells (PSC), and carried out co-culture experiments using cerulein and Transwell co-culture chambers. Experimental steps: First, we inoculated mouse pancreatic acinar cells with or without cerulein treatment in the lower chamber of the Transwell co-culture chamber. After culturing for 12 h, we replaced the culture medium with new medium without cerulein. Then, we transferred the upper chamber, in which mouse pancreatic stellate cells have been pre-inoculated, to the lower chamber and continued culturing for 12 h. (D) The protein expression levels of α -SMA, COL1A1, and CXCL1 in PSC co-cultured with pancreatitis cell models or acinar cells of the normal control group under hypoxic and nonhypoxic conditions. (E) The mRNA expression levels of IL-1 β , TNF- α , and IL-6 in acinar cells of the pancreatitis cell model or the normal control group under hypoxic and nonhypoxic conditions. (F) The effects of si-P65 and/or si-HIF-1 α on the expression of CXCL1 in human pancreatic stellate cells under hypoxic conditions

Supplementary file 2. Figure 2: (A) Change trend of transcription factor motif AUC values of three fibroblast sub-groups. (B) Fibroblasts 2 in AP group highly expressed chemokines such as CXCL1, CXCL2, CCL2, and CCL7 compared with NC group. (C) KEGG enrichment of module genes in the yellow module with the strongest correlation with fibroblasts 3.

Supplementary file 3. Figure 3: (A) The enrichment level of acinar cells in the control group and in AP. (B) The expression of CXCL1 mRNA in each group after acinar cells were stimulated by cerulein

Supplementary file 4. Figure 4: Uncropped pictures of Western blot

Supplementary file 5. Figure 5: Uncropped pictures of Western blot.

Supplementary file 6. Figure 6: Uncropped pictures of Western blot

Supplementary file 7. Figure 7: Uncropped pictures of Western blot.

Supplementary file 8. Table 1: Histopathologic Scoring Criteria.

Author contributions

Q.W., L.W., T.L., and D.X. conceived and designed this study, performed data analysis, organized figures, and wrote the manuscript. Unless otherwise stated, Q.W., X.Z., and C.H. designed and conducted all experiments, and interpreted and analyzed all sequencing data. Z.L. and Y.Z. were responsible for the mouse experiments. X.L. was responsible for collecting blood samples. T.L. and Z.D. provided technical assistance for in vivo experiments.

Funding

This research was funded by the National Natural Science Foundation of China (no. 82170654), the Key Research and Development Program of Heilongjiang Province (no. 2022ZX06C06), the National Key Research and Development Program of China (2017YFA0104902), and grants from the Taishan Scholars Program of Shandong Province (grant no. tstp20221158), National Natural Science Foundation of China (grant no. 82073200 and 81874178), the 74th batch of general projects of China Postdoctoral Science Foundation (no. 2023M742121), and Postdoctoral Innovation Project of Shandong Province (project no. SDCX-ZG-202400052).

Availability of data and material

All data are public. Single-cell sequencing data will be uploaded to the GEO database (GSE279876) and can also be obtained by contacting the corresponding author.

Declarations

Ethics approval and consent to participate

The animal experiments involved in this study were approved by the Animal Ethics Committee of the First Affiliated Hospital of Harbin Medical University on 15 May 2021 (no. 2021091). All animal experiments comply with the guidelines of the International Council for Laboratory Animal Science. The blood samples of pancreatitis patients used in this study were approved by the Ethics Committee of the First Affiliated Hospital of Harbin Medical University on 3 February 2023 (no. HMU-SRER-202323). All participants have been informed. All the research was conducted in accordance with the Declaration of Helsinki.

Consent for publication

Not applicable.

Competing interests

No benefits in any form have been received or will be received from a commercial party related directly or indirectly to the subject of this article.

Received: 1 November 2024 Accepted: 17 April 2025

Published online: 07 May 2025

References

1. Mederos MA, Reber HA, Girgis MD. Acute pancreatitis: a review. *JAMA*. 2021;325(4):382–90.
2. Ji L, Wang ZH, Zhang YH, Zhou Y, Tang DS, Yan CS, et al. ATG7-enhanced impaired autophagy exacerbates acute pancreatitis by promoting regulated necrosis via the miR-30b-5p/CAMKII pathway. *Cell Death Dis*. 2022;13(3):211.
3. Lou D, Shi K, Li HP, Zhu Q, Hu L, Luo J, et al. Quantitative metabolic analysis of plasma extracellular vesicles for the diagnosis of severe acute pancreatitis. *J Nanobiotechnology*. 2022;20(1):52.
4. Peng C, Li Z, Yu X. The role of pancreatic infiltrating innate immune cells in acute pancreatitis. *Int J Med Sci*. 2021;18(2):534–45.
5. Wan J, Yang X, Ren Y, Li X, Zhu Y, Haddock AN, et al. Inhibition of miR-155 reduces impaired autophagy and improves prognosis in an experimental pancreatitis mouse model. *Cell Death Dis*. 2019;10(4):303.
6. Banks PA, Bollen TL, Dervenis C, Gooszen HG, Johnson CD, Sarr MG, et al. Classification of acute pancreatitis—2012: revision of the Atlanta classification and definitions by international consensus. *Gut*. 2013;62(1):102–11.
7. Garg PK, Singh VP. Organ failure due to systemic injury in acute pancreatitis. *Gastroenterology*. 2019;156(7):2008–23.
8. Cassatella MA. Neutrophil-derived proteins: selling cytokines by the pound. *Adv Immunol*. 1999;73:369–509.
9. Wan J, Ren Y, Yang X, Li X, Xia L, Lu N. The role of neutrophils and neutrophil extracellular traps in acute pancreatitis. *Front Cell Dev Biol*. 2020;8:565758.
10. Chen G, Xu F, Li J, Lu S. Depletion of neutrophils protects against L-arginine-induced acute pancreatitis in mice. *Cell Physiol Biochem*. 2015;35(6):2111–20.
11. Gukovskaya AS, Vaquero E, Zaninovic V, Gorelick FS, Lulis AJ, Brennan ML, et al. Neutrophils and NADPH oxidase mediate intrapancreatic trypsin activation in murine experimental acute pancreatitis. *Gastroenterology*. 2002;122(4):974–84.
12. Sandoval D, Gukovskaya A, Reavey P, Gukovsky S, Sisk A, Braquet P, et al. The role of neutrophils and platelet-activating factor in mediating experimental pancreatitis. *Gastroenterology*. 1996;111(4):1081–91.
13. Yu C, Merza M, Luo L, Thorlacius H. Inhibition of Ras signalling reduces neutrophil infiltration and tissue damage in severe acute pancreatitis. *Eur J Pharmacol*. 2015;746:245–51.
14. Montecucco F, Mach F, Lenglet S, Vonlaufen A, Gomes Quinderé AL, Pelli G, et al. Treatment with Evasin-3 abrogates neutrophil-mediated inflammation in mouse acute pancreatitis. *Eur J Clin Invest*. 2014;44(10):940–50.
15. Shields CJ, Winter DC, Redmond HP. Lung injury in acute pancreatitis: mechanisms, prevention, and therapy. *Curr Opin Crit Care*. 2002;8(2):158–63.
16. Pilszczek FH, Salina D, Poon KK, Fahey C, Yipp BG, Sibley CD, et al. A novel mechanism of rapid nuclear neutrophil extracellular trap formation in response to *Staphylococcus aureus*. *J Immunol*. 2010;185(12):7413–25.
17. Huang J, Hong W, Wan M, Zheng L. Molecular mechanisms and therapeutic target of NETosis in diseases. *Med-Comm*. 2022;3(3): e162.
18. Adrover JM, Aroca-Crevillén A, Crainiciuc G, Ostos F, Rojas-Vega Y, Rubio-Ponce A, et al. Programmed “disarming” of the neutrophil proteome reduces the magnitude of inflammation. *Nat Immunol*. 2020;21(2):135–44.
19. Merza M, Hartman H, Rahman M, Hwaiz R, Zhang E, Renström E, et al. Neutrophil extracellular traps induce trypsin activation, inflammation, and tissue damage in mice with severe acute pancreatitis. *Gastroenterology*. 2015;149(7):1920–1931.e8.
20. Zhang H, Wang Z, Li J, Jia Y, Li F. Timing, initiation and function: An in-depth exploration of the interaction network among neutrophil extracellular traps related genes in acute pancreatitis. *Int Immunopharmacol*. 2024;141:112923.
21. Habtezion A. Inflammation in acute and chronic pancreatitis. *Curr Opin Gastroenterol*. 2015;31(5):395–9.
22. Kolaczowska E, Kuberski P. Neutrophil recruitment and function in health and inflammation. *Nat Rev Immunol*. 2013;13(3):159–75.
23. Linde IL, Prestwood TR, Qiu J, Pilarowski G, Linde MH, Zhang X, et al. Neutrophil-activating therapy for the treatment of cancer. *Cancer Cell*. 2023;41(2):356–372.e10.
24. Liu Y, Cui H, Mei C, Cui M, He Q, Wang Q, et al. Sirtuin4 alleviates severe acute pancreatitis by regulating HIF-1 α /HO-1 mediated ferroptosis. *Cell Death Dis*. 2023;14(10):694.
25. Schmidt J, Rattner DW, Lewandrowski K, Compton CC, Mandavilli U, Knoefel WT, et al. A better model of acute pancreatitis for evaluating therapy. *Ann Surg*. 1992;215(1):44–56.
26. Butler A, Hoffman P, Smibert P, Papalexis E, Satija R. Integrating single-cell transcriptomic data across different conditions, technologies, and species. *Nat Biotechnol*. 2018;36(5):411–20.
27. Han X, Wang R, Zhou Y, Fei L, Sun H, Lai S, et al. Mapping the Mouse Cell Atlas by Microwell-Seq. *Cell*. 2018;172(5):1091–1107.e17.
28. Fairfax KA, Bolden JE, Robinson AJ, Lucas EC, Baldwin TM, Ramsay KA, et al. Transcriptional profiling of eosinophil subsets in interleukin-5 transgenic mice. *J Leukoc Biol*. 2018;104(1):195–204.
29. Apte MV, Park S, Phillips PA, Santucci N, Goldstein D, Kumar RK, et al. Desmoplastic reaction in pancreatic cancer: role of pancreatic stellate cells. *Pancreas*. 2004;29(3):179–87.
30. Haber PS, Keogh GW, Apte MV, Moran CS, Stewart NL, Crawford DH, et al. Activation of pancreatic stellate cells in human and experimental pancreatic fibrosis. *Am J Pathol*. 1999;155(4):1087–95.
31. Casini A, Galli A, Pignatola P, Frulloni L, Grappone C, Milani S, et al. Collagen type I synthesized by pancreatic periacinar stellate cells (PSC) co-localizes with lipid peroxidation-derived aldehydes in chronic alcoholic pancreatitis. *J Pathol*. 2000;192(1):81–9.
32. Bachem MG, Schneider E, Gross H, Weidenbach H, Schmid RM, Menke A, et al. Identification, culture, and characterization of pancreatic stellate cells in rats and humans. *Gastroenterology*. 1998;115(2):421–32.

33. Rius J, Guma M, Schachtrup C, Akassoglou K, Zinkernagel AS, Nizet V, et al. NF- κ B links innate immunity to the hypoxic response through transcriptional regulation of HIF-1 α . *Nature*. 2008;453(7196):807–11.
34. Dey A, Prabhudesai S, Zhang Y, Rao G, Thirugnanam K, Hossen MN, et al. Cystathione β -synthase regulates HIF-1 α stability through persulfidation of PHD2. *Sci Adv*. 2020. <https://doi.org/10.1126/sciadv.aaz8534>.
35. Lin X, Lei Y, Pan M, Hu C, Xie B, Wu W, et al. Augmentation of scleral glycolysis promotes myopia through histone lactylation. *Cell Metab*. 2024;36(3):511–525.e7.
36. Awla D, Abdulla A, Zhang S, Roller J, Menger MD, Regnér S, et al. Lymphocyte function antigen-1 regulates neutrophil recruitment and tissue damage in acute pancreatitis. *Br J Pharmacol*. 2011;163(2):413–23.
37. Abdulla A, Awla D, Thorlacius H, Regnér S. Role of neutrophils in the activation of trypsinogen in severe acute pancreatitis. *J Leukoc Biol*. 2011;90(5):975–82.
38. Korhonen JT, Dudeja V, Dawra R, Kubes P, Saluja A. Neutrophil extracellular traps provide a grip on the enigmatic pathogenesis of acute pancreatitis. *Gastroenterology*. 2015;149(7):1682–5.
39. Xiong G, Chen Z, Liu Q, Peng F, Zhang C, Cheng M, et al. CD276 regulates the immune escape of esophageal squamous cell carcinoma through CXCL1-CXCR2 induced NETs. *J Immunother Cancer*. 2024. <https://doi.org/10.1136/jitc-2023-008662>.
40. Zimmermann A, Gloor B, Kappeler A, Uhl W, Friess H, Büchler MW. Pancreatic stellate cells contribute to regeneration early after acute necrotising pancreatitis in humans. *Gut*. 2002;51(4):574–8.
41. Lugea A, Nan L, French SW, Bezerra JA, Gukovskaya AS, Pandolfi SJ. Pancreas recovery following cerulein-induced pancreatitis is impaired in plasminogen-deficient mice. *Gastroenterology*. 2006;131(3):885–99.
42. Hama K, Ohnishi H, Aoki H, Kita H, Yamamoto H, Osawa H, et al. Angiotensin II promotes the proliferation of activated pancreatic stellate cells by Smad7 induction through a protein kinase C pathway. *Biochem Biophys Res Commun*. 2006;340(3):742–50.
43. Masamune A, Satoh M, Kikuta K, Suzuki N, Shimosegawa T. Endothelin-1 stimulates contraction and migration of rat pancreatic stellate cells. *World J Gastroenterol*. 2005;11(39):6144–51.
44. Kuno A, Yamada T, Masuda K, Ogawa K, Sogawa M, Nakamura S, et al. Angiotensin-converting enzyme inhibitor attenuates pancreatic inflammation and fibrosis in male Wistar Bonn/Kobori rats. *Gastroenterology*. 2003;124(4):1010–9.
45. Masamune A, Kikuta K, Suzuki N, Satoh M, Satoh K, Shimosegawa T. A c-Jun NH2-terminal kinase inhibitor SP600125 (anthra[1,9-cd]pyrazole-6 (2H)-one) blocks activation of pancreatic stellate cells. *J Pharmacol Exp Ther*. 2004;310(2):520–7.
46. Huang Q, Zhan L, Cao H, Li J, Lyu Y, Guo X, et al. Increased mitochondrial fission promotes autophagy and hepatocellular carcinoma cell survival through the ROS-modulated coordinated regulation of the NF- κ B and TP53 pathways. *Autophagy*. 2016;12(6):999–1014.
47. Wang L, Huang J, Zhang R, Zhang M, Guo Y, Liu Y, et al. Cullin 5 aggravates hypoxic pulmonary hypertension by activating TRAF6/NF- κ B/HIF-1 α /VEGF. *IScience*. 2023;26(11):108199.
48. Chen Q, Tang L, Zhang Y, Wan C, Yu X, Dong Y, et al. STING up-regulates VEGF expression in oxidative stress-induced senescence of retinal pigment epithelium via NF- κ B/HIF-1 α pathway. *Life Sci*. 2022;293:120089.
49. Wang XH, Xu S, Zhou XY, Zhao R, Lin Y, Cao J, et al. Low chorionic villous succinate accumulation associates with recurrent spontaneous abortion risk. *Nat Commun*. 2021;12(1):3428.
50. Janbandhu V, Tallapragada V, Patrick R, Li Y, Abeygunawardena D, Humphreys DT, et al. Hif-1 α suppresses ROS-induced proliferation of cardiac fibroblasts following myocardial infarction. *Cell Stem Cell*. 2022;29(2):281–297.e12.
51. Becker LM, O'Connell JT, Vo AP, Cain MP, Tampe D, Bizarro L, et al. Epigenetic reprogramming of cancer-associated fibroblasts deregulates glucose metabolism and facilitates progression of breast cancer. *Cell Rep*. 2020;31(9):107701.
52. Wang F, Chen L, Kong D, Zhang X, Xia S, Liang B, et al. Canonical Wnt signaling promotes HSC glycolysis and liver fibrosis through an LDH-A/HIF-1 α transcriptional complex. *Hepatology*. 2024;79(3):606–23.

Publisher's Note

Springer Nature remains neutral with regard to jurisdictional claims in published maps and institutional affiliations.